Article

Femtomolar hydrogen sulfide detection via hybrid small-molecule nano-arrays

Xing Xing[1,2,3], Luyan Wu[4], Yuchen Zhang[1], Jiahao Pan[1], Yusuke Ishigaki [5], Huaqing Xie[2], Takanori Suzuki [5], Deju Ye [4], Jianhua Zhang[6], Weihua Zhang [1] & Zhenda Lu [1,3,4] ✉

Early disease diagnosis hinges on the sensitive detection of signaling molecules. Among these, hydrogen sulfide (H_2S) has emerged as a critical player in cardiovascular and nervous system signaling. On-chip immunoassays, particularly nanoarray-based interfacial detection, offer promising avenues for ultra-sensitive analysis due to their confined reaction volumes and precise signal localization. Beyond the DNA or protein biomolecules array, this work presents a promising hybrid small molecule nano-array for H_2S detection, using the power of dual molecules: a dye for fluorescence emission and a quencher with specific H_2S reactivity. Upon H_2S interaction, the quenched fluorescence reignites, creating an easily detectable array of bright spots. The molecule nano-array sensor shows exceptional responses to H_2S over 8 magnitudes of dynamic range from 1 fM to 0.1 μM, with a remarkable detection limit of 1 fM, just using a 10 μL solution. This H_2S detection method has the potential to significantly improve bioassay platforms, and the hybrid small-molecule nano-arrays we developed could be a valuable tool for advancing signaling molecule detection.

Hydrogen sulfide (H_2S) has been recognized as a signaling molecule in the cardiovascular and nervous systems, making its accurate detection vital for diagnosing and managing related diseases[1–5]. While baseline H_2S levels hover around micromolar, detecting even lower concentrations holds immense promise, offering a previous window for the early-stage illness diagnosis and intervention before symptoms manifest[6–17].

To meet the demand, a recent study introduced $F1^{2+}$, a bis(pentafluorophenyl)-substituted organic π-electron structure[18,19]. $F1^{2+}$ boasts impressive characteristics: rapid reaction kinetics to H_2S with excellent specificity, minimizing false positives[18]. Utilizing this remarkable molecule, researchers achieved an impressive detection limit of 0.1 μM endogenous H_2S in vitro, showing its potential for

sensitive biomedical applications[18]. However, pushing the boundaries of detection even further demands innovative approaches.

On the other hand, micro-arrays have long been an invaluable tool for rapid, high-throughput, and sensitive analysis[20–27]. Their well-arranged molecular spots offer enhanced accuracy and quantitative precision, resulting in a clear contrast to the random molecules. Advancements in micro-nano fabrication have yielded dense micro-arrays, exceeding 1000 spots per square millimeter[22]. But nano-arrays, offer even higher density and miniaturized reaction spaces[26,28,29]. Imagine hundreds of reaction tests can occur in the area of a single conventional microarray spot, enabling the performance of ultra-sensitive detection, rapid analysis, and small sample volumes.

[1]College of Engineering and Applied Sciences, Jiangsu Key Laboratory of Artificial Functional Materials, Nanjing University, Nanjing, China. [2]School of Energy and Materials, Shanghai Thermophysical Properties Big Data Professional Technical Service Platform, Shanghai Engineering Research Center of Advanced Thermal Functional Materials, Shanghai Polytechnic University, Shanghai, China. [3]School of the Environment, Research Center for Environmental Nanotechnology (ReCENT), Nanjing University, Nanjing, China. [4]State Key Laboratory of Analytical Chemistry for Life Science, School of Chemistry and Chemical Engineering, Nanjing University, Nanjing, China. [5]Department of Chemistry, Faculty of Science, Hokkaido University, Sapporo, Japan. [6]N.O.D topia (GuangZhou) Biotechnology Co., Ltd., Simpcare (GuangZhou) Biotechnology Co. Ltd., Guangzhou, China. ✉e-mail: luzhenda@nju.edu.cn

However, precisely positioning and integrating multiple molecules on the nanoscale remains a formidable challenge[30-34]. While existing nano-arrays focus on larger biomolecules like DNA and proteins, the small-molecule nano-arrays, are rarely reported[35-41]. This is, in part, due to the inherent nature of small molecules – they are difficult to manipulate, lack strong bonds with the substrate, and are hard to detect.

Here, we present a molecule nano-array fabrication method based on a modified nano-xerography technique[42-47], precisely co-assembling Rhodamine B (RB) dye and $F1^{2+}$ molecules into nano-arrays, with a spot size of ~100 nm and a spot-to-spot pitch of 3–5 μm. The spot, as a nanoreactor, is capable of capturing trace amounts of H_2S from test solutions, decomposing the quencher $F1^{2+}$ molecules, and then reigniting the RB fluorescence. This approach at least has several key advantages: 1) ultra-sensitive detection: nanoscale reaction areas make the array quantitatively responsive to trace amounts of H_2S, reaching detection limits of 1 fM. Also, the small size of the spots allows for quick and real-time detection, which is crucial in biological diagnostics. 2) broad-range detection: different data processing methods, Intensity integral (INTEN) and Number counting (NUMB), depending on the analyte concentration can be applied, making a detection range of H_2S that spans over 8 orders of magnitude, from 1 fM to 0.1 μM. 3) specific detection: taking advantage of the chemical affinity system, the high H_2S specificity of $F1^{2+}$ ensures sensitive and reliable detection.

Combining the power of $F1^{2+}$ and molecule nano-arrays, this innovative approach paves a new way of ultra-sensitive H_2S detection. Moreover, this kind of molecule nano-arrays can extend to other molecular fluorescence probe systems, making it universal to develop an innovative analysis method of the small signaling molecules in biological systems.

Results

Characteristics of hybrid molecule nano-array

The molecule nano-array sensor, which is schematically shown in Fig. 1a, comprises a spot of hybrid molecules with each spot diameter of ~100 nm (Supplementary Fig. S1). Among them, the hybrid molecules consist of fluorescence-quencher molecules ($F1^{2+}$), dye molecule RB, and cyclodextrin. $F1^{2+}$ molecule has wide fluorescence absorption capacity in the visible light range, especially in the 500–650 and 700–900 nm, which covers the excitation and emission wavelength of most dye molecules. RB dye molecule is selected as the fluorescence agent, a common dye molecule with absorption and emission center wavelengths of 530 nm and 590 nm, respectively, that can be quenched by $F1^{2+}$ molecule effectively. β-Cyclodextrin (CD) was used as a space barrier to prevent aggregation-caused quenching (ACQ) of dye molecules. The CD and RB inclusion complexes were investigated using circular dichroism (Supplementary Fig. S2), which indicated 1:1 compound was formed. The absorption spectra of the separated three molecules and their combination were shown in Supplementary Fig. S3a, which were characterized by spin-coating the corresponding molecules onto a cover glass. $F1^{2+}$ can be quickly reduced to an F2 molecule by H_2S (Fig. 1b), which has almost no absorption in the visible light range (Supplementary Fig. S3b). The absorption spectra of $F1^{2+}$ and $F1^{2+}$/RB/CD on a substrate were evaluated over 7 days in air (Supplementary Fig. S4), showing their exceptional air stability.

Based on this reaction platform, we printed the hybrid molecules with certain proportions into nano-arrays on the substrate by the modified nanoxerography method we developed[42,43]. At each spot, the RB fluorescence emitted is quenched by $F1^{2+}$ molecules, so that the nano-arrays before reacting with H_2S showed very weak fluorescence. When $F1^{2+}$ is decomposed by H_2S molecules, the fluorescence of the RB regenerates, which can be easily imaged by a wide-field fluorescence microscope. As depicted in Supplementary Fig. S5, only the NaHS solution illuminated the nanoarray while other reductants and ROS exhibited few changes in fluorescence intensity. This investigation highlights the excellent specificity of our hybrid molecular nanoarray towards H_2S detection.

The fluorescence change of each spot in the nano-array correlates with the H_2S concentration. We utilize an intensity integral (INTEN) and number counting (NUMB) method to quantify the fluorescence activities on the spots at high and low H_2S concentrations, respectively (Fig. 1c)[48,49]. The INTEN method surveys all the spots in the nanoarray and integrates the fluorescence intensity, which can detect H_2S concentration from 0.3 pM to 0.1 μM. At low concentrations, only parts of the spots have measurable fluorescence changes (defined as "on"). The
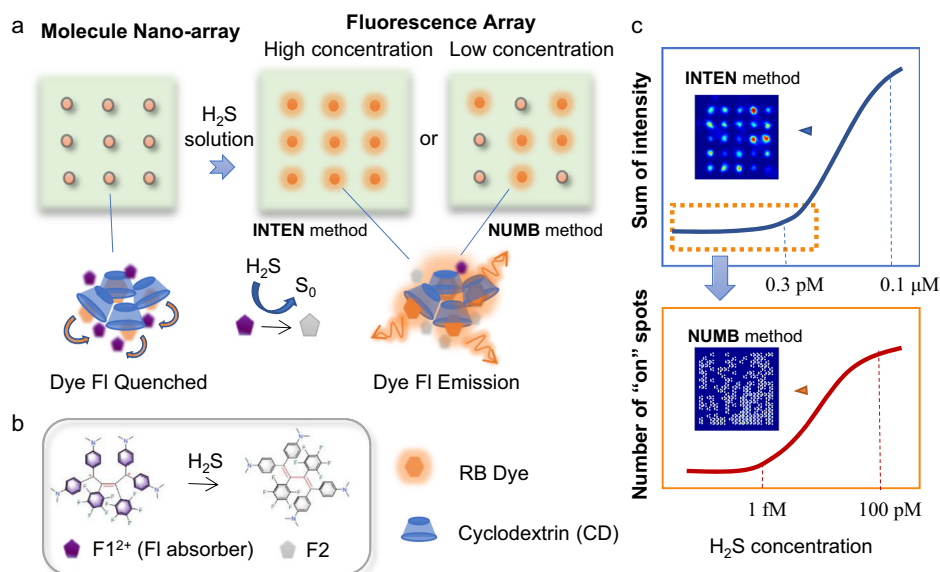

Fig. 1 | Illustration of highly sensitive H_2S detection via a hybrid molecule nano-array. a The design of a hybrid molecule nano-array for H_2S detection, involving $F1^{2+}$, RB, and cyclodextrin (CD) molecules. During the process of H_2S detection, the spots within the molecule array transition from the fluorescence "off" state to an "on" state. By integrating the fluorescence intensity (INTEN method) at high concentrations or counting the number of the "on" spots (NUMB method), the correlation with H_2S concentration can be established. **b** The chemical equation of $F1^{2+}$ to F2 reduced by H_2S. **c** The typical fluorescent image of the array and the corresponding correlation spots obtained by INTEN and NUMB methods at high H_2S concentration and low concentration respectively.
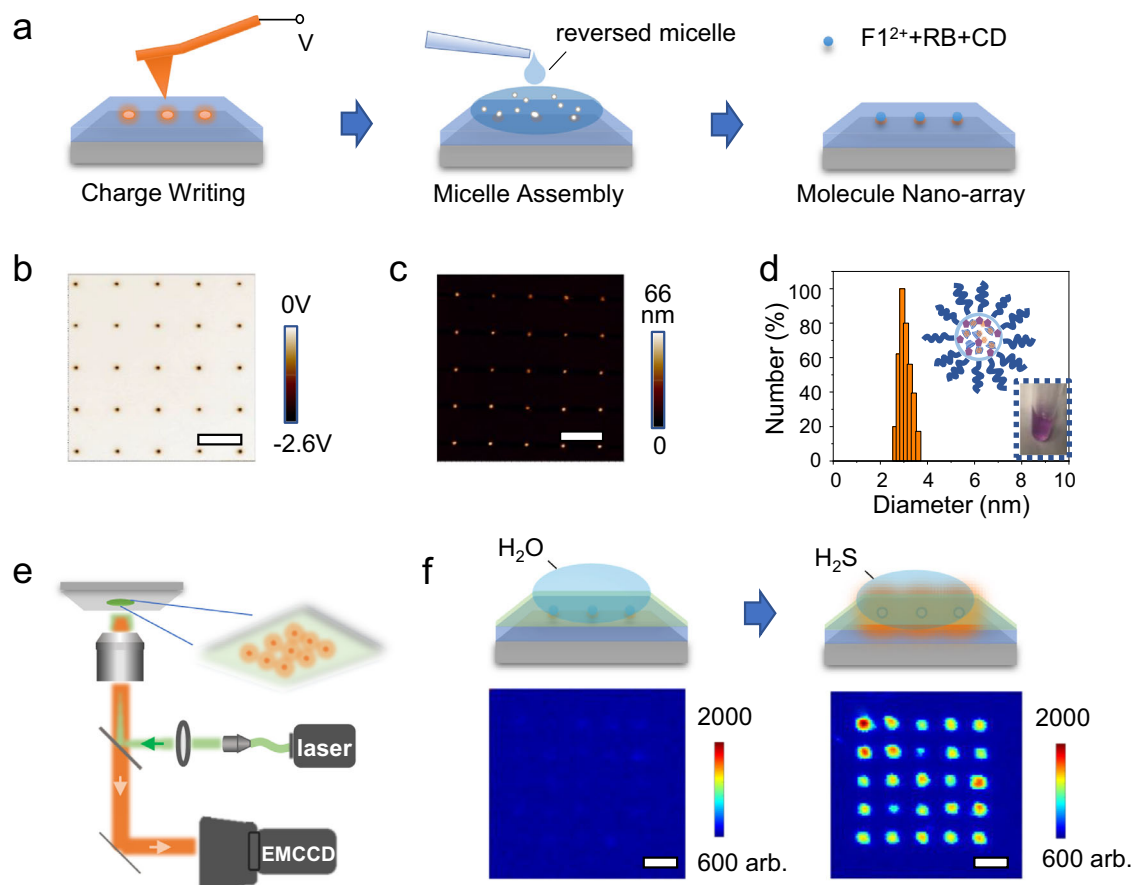
Fig. 2 | Fabrication and characterization of hybrid molecule nano-arrays.
a Schematic illustration of fabricating hybrid molecule nano-array using modified nanoxerography method, which involves surface charge writing, reversed-micelle preparation, and site-specific assembly by electrical trapping. **b** Electric potential map after writing a 5 × 5 charge array on the substrate. Scale bar, 5 μm. **c** AFM height map of the hybrid molecule nano-array, with an average height of 50 nm. Scale bar, 5 μm. **d** Dynamic light scattering (DLS) result of reversed-micelles, with the statistic size in dispersion around 3 nm. Inset is a photograph of the micelle dispersion in a test tube. **e** Scheme of the fluorescence array imaging reader. A homemade inverted widefield microscope is equipped with a fiber-coupled 532 nm continuous-wave laser diode and a sensitive Electron Multiplying Charge-Coupled Device (EMCCD) camera. **f** Schematic illustration of H_2S detection, and corresponding PL images of the hybrid molecule array after incubation with water (10 μL) and H_2S solution (10 μL, 0.1 μM). Scale bar, 5 μm.

NUMB method counts the separated "on" spots, showing a good correlation with the H_2S concentration in the range of 1 fM to 100 pM, two orders of magnitude lower than that of INTEN method. The detailed configurations of INTEN and NUMB methods are listed in the Experimental Section.

As a comparison, we evaluated the sensing performance of $F1^{2+}$/RB/CD micelles in solution. The results, as shown in Supplementary Fig. S6, demonstrate a detection range of 10 nM to 1 μM for NaHS. Compared to solution-based methods, the nanoarray platform clearly offers a wider response range and lower detection limit.

Preparation of hybrid molecule nano-array
The molecule nano-array was fabricated by the modified nanoxerography method we had reported previously[42,43]. The typical procedures are schematically shown in Fig. 2a. First, a local surface charge array was written on the substrate by controlling a conductive atomic force microscopy (AFM) probe to apply high voltage (~−80V), which can generate −2.4 V charge potential on the substrate, as proved by the Kelvin probe force microscopy (KPFM) potential maps in Fig. 2b. Then, $F1^{2+}$, RB, and CD molecules were dissolved in water as a dispersed phase to form water-in-oil reverse micelles, with isooctane as a continuous phase and Sodium bis(2-ethylhexyl) sulfosuccinate (AOT) as a surfactant. The micelles loaded with $F1^{2+}$, RB, and CD were spin-coated on the substrate. During this process, the molecules would be enriched and adsorbed onto the charged array. In the uncharged area, the

perfluorinated substrate (CYTOP) could effectively avoid non-specific adsorption due to its ultra-low surface energy. The main driving force for micelle assembly was dielectrophoretic interactions between micelles and charged spots on the substrate[50,51]. As shown in AFM height map (Fig. 2c), a 5 × 5 molecular nano-array was successfully assembled with less nonspecific adsorption with a spot size of ~200 nm and a spacing of 5 μm, The micelle dispersion was characterized by dynamic light scattering (DLS) and Zeta potential measurement. The DLS result (Fig. 2d) demonstrates the average micelle size in solution is around 3 nm, which is consistent with the results previously reported in the literature[42,52]. The zeta potential is around −31.1 ± 11.0 mV, indicating the strong negative charge and the good stability of the micelles.

To investigate the steric spacer effect of β-cyclodextrin (CD) in the hybrid molecular system, we prepared RB micelles and RB/CD mixture micelles (1:1 molar ratio) and assembled them onto charged spots with identical surface potential. As expected, no fluorescence array was observed, attributed to aggregation-caused quenching (ACQ) of RB molecules (Supplementary Fig. S7a). Upon the addition of CD, a robust fluorescence nano-array emerged (Supplementary Fig. S7b). Subsequently, RB/CD was combined with the quencher molecule $F1^{2+}$ to form the final $F1^{2+}$/RB/CD system (1:1:2 molar ratio). The average fluorescence intensity of the spots decreased significantly, reaching only 9% compared to the case without $F1^{2+}$ molecules (Supplementary Fig. S7c).

The molar ratio of F1²⁺/RB/CD is a critical factor influencing detection range and sensitivity. As demonstrated in Supplementary Fig. S8, a 2:1 F1²⁺/RB ratio optimizes these parameters. A higher F1²⁺ proportion (9:1 F1²⁺/RB) leads to increased NaHS consumption and limited fluorescence change due to insufficient RB. Conversely, a lower F1²⁺ proportion restricts the detection range. As the result, this F1²⁺/RB/CD hybrid molecular system (2:1:1 molar ratio) was chosen for subsequent micro-area fluorescence detection.

Typical PL images of 5 × 5 nano-array before and after reacting with H₂S solution are shown in Fig. 2f. After 2 min of the reaction (Supplementary Fig. S9), the fluorescence intensity of each hybrid molecule spot ranges from 300 to over 15,000 arbitrary units (a.u.), compared to less than 290 a.u. of the negative controls (incubated with water). The fluorescence intensity on each spot is enhanced more than 50 times. These results clearly demonstrate the enormous potential of the nano-array in ultra-sensitive small molecule detection.

It's worth mentioning that this hybrid molecule nanoarray platform is also applicable to other dye molecules for detecting H₂S. CY-NH₂ dye (em 690 nm) and Luciferin dye (em 510 nm) were selected to investigate the versatility of this hybrid molecule nanoarray platform (Supplementary Fig. S10). However, RB dye was selected due to its optimal spectral overlap with F1²⁺ (Supplementary Fig. S11) and superior photophysical properties, including high fluorescence quantum yield, light stability, pH insensitivity, and molar extinction coefficient, making it well-suited for detection applications.

Quantitatively H₂S detection at high concentrations using INTEN method

We quantificationally investigated the luminescence response of the hybrid molecule nano-array toward H₂S. 10 μL of sodium hydrosulfide (NaHS) aqueous solution ranging from 0.1 fM to 1 μM were tested by the hybrid molecule nano-arrays (5 × 5 square spots). The conversion of NaHS to H₂S is a hydrolysis process that detail chemical equilibrium has been represented in Supplementary Information Note S1. Figure 3a shows the fluorescence images of the nano-array after sulfide assay from 10 pM to 1 μM. The images related to the other concentrations are shown in Supplementary Fig. S12. It is clear that the fluorescence intensity on each spot have a positive correlation with the concentration. All the spots are illuminated when the concentration is above 100 pM, on the contrary, only parts of spots are detectable in the images below 10 pM. To quantitatively analyze the correlation, we read out the fluorescence intensity of each spot. (Detailed information are shown in the Method Section, and Supplementary Figs. S13 and S14). If the intensity is larger than that before NaHS assay, we considered it an illuminated spot ("on" spot). The intensity sum of all the "on" spot versus corresponding concentration were plotted (Fig. 3b), noted as INTEN method. The plot is fitted with the well-established four-parameter logistic function curve (4-PL fitting), showing a good dynamic detection range over 5 magnitudes, from 300 fM to 1 μM. The linear range after logit transformation was between 100 pM and 100 nM, in which the spots are all reignites.

Quantitatively H₂S detection at low concentrations using NUMB method

As the NaHS concentration was below 10 pM, the sum of fluorescence intensity of the "on" spot is relatively low to quantitative analysis, and parts of the spots hold the "off" state (Supplementary Fig. S12). Due to insufficient hydrogen sulfide exposure for all spots, fluorescence changes may not be detected within 2 min, especially at low concentrations. In view of this, we counted "on" spot numbers, and correlated them with the NaHS concentrations, noted as NUMB method. To get more reliable results at low concentration of NaHS, we increased the spot number to 400 by designing a 20 × 20 array pattern (Fig. 4 and Supplementary Fig. S15). NaHS solutions with concentrations from 0.1 fM to 1 nM were prepared. Figure 4a shows the fluorescence images corresponding to the concentration from 1fM to 100 pM, and all the "on" spots marked with circles. The 20 × 20 molecule nano-array showed the NaHS detection limit of around 70 fM using INTEN method (Fig. 4b). In comparison, the detection limit is about 300 fM with the same method when utilizing the 5×5 nanoarray, indicating more spots can lead to a lower detection limit.

The images were further characterized by NUMB method to extend the NaHS detection limit to an even lower concentration (Fig. 4b). After 4-PL fitting, a good correlation between the number of "on" spots and the concentration of NaHS from 1 fM to 100 pM is demonstrated with the R^2 value of 0.99 (Supplementary Table S1), indicating exceptional dynamic detection range. The detection limit has been reduced by about 2 orders of magnitude, compared to the INTEN method.
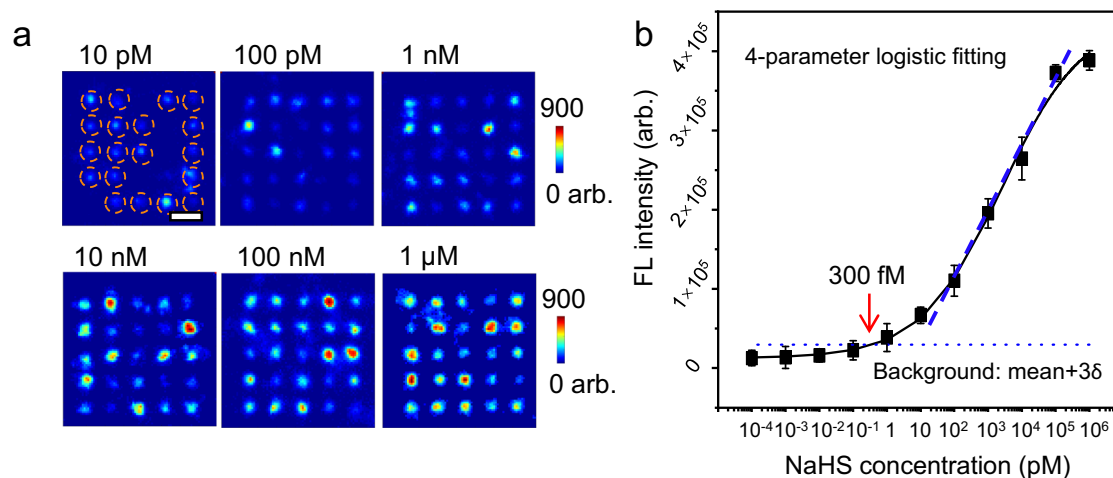

Fig. 3 | H₂S detection at high concentration using INTEN method. a PL images of serial NaHS concentration in 10 pM, 100 pM, 1 nM, 10 nM, 100 nM, and 1 μM in the 5 × 5 nano-assay. The images of other concentrations (from 0.1 fM to 1 pM) are shown in Supplementary Fig. S12. Scale bar, 5 μm. **b** The working curve of NaHS tested on the nanoarray using the INTEN method. The black line shows the fitting result by the 4-parameter logistic regression model. The blue dotted line represents the background levels, which are defined as the mean luminescence intensity of negative controls with a three-fold standard deviation. The fitting parameters are listed in Supplementary Table S1. The blue dash line shows the linear regression after logit transformation of the method. Error bars indicate the standard deviation from three replicate experiments.
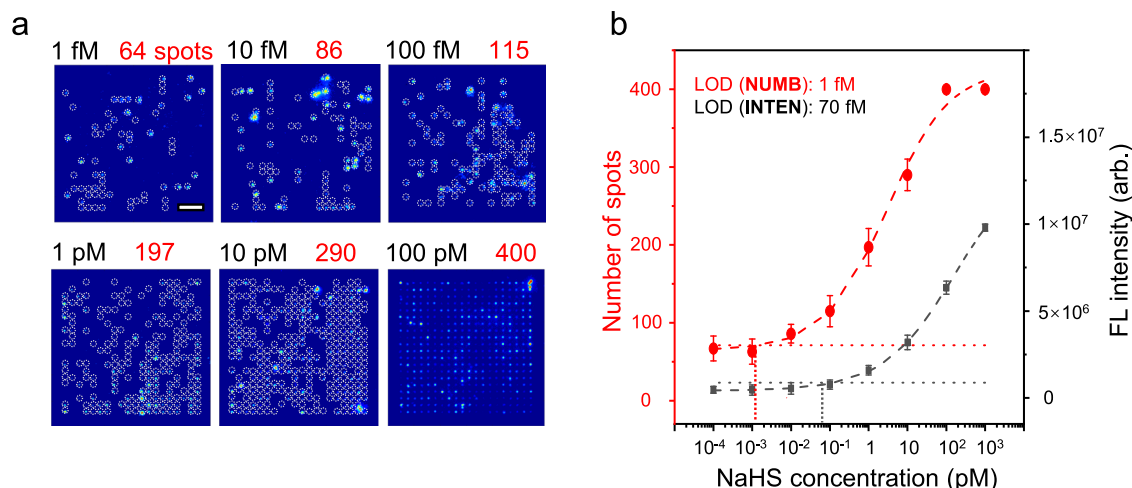
Fig. 4 | H₂S detection at low concentration using NUMB method. a PL images of serial NaHS concentration in 1 fM, 10 fM, 100 fM, 1 pM, 10 pM and 100 pM in the assay of 20 × 20 molecules nano-array. Scale bar, 9 μm. **b** The fitting results of the NUMB and INTEN methods. The 4-parameter logistic regression model yields an LOD of 1 fM in the NUMB method and 70 fM in the INTEN method. The dotted line represents the background levels, which are defined as the mean luminescence intensity of negative controls with a three-fold standard deviation. The fitting parameters are listed in Supplementary Table S1. Error bars indicate the standard deviation from three replicate experiments.

Combined with the results from INTEN method at high NaHS concentrations and NUMB method at low NaHS concentrations, this hybrid molecule nano-array platform has achieved the detection dynamic range from 1 fM to 0.1 μM, about 8 orders of magnitudes of response. This is a significant improvement in detection range and detection limit compared to the existing method for signaling small molecules.

Discussion

We have developed a hybrid molecule nano-array sensor and implemented it for the highly sensitive detection of hydrogen sulfide. The nano-array features a small reaction volume, enabling a specific response from the F1²⁺ molecule designed for H₂S detection. With its high-sensitivity turn-on fluorescence detection mechanism, this nano-array achieves an exceptional detection limit of 1 fM using just a 10 μL solution. Furthermore, it exhibits a broad detection dynamic range spanning 8 orders of magnitudes. The outstanding performance of this nano-array is attributed to the robust nanoxerography technique and the use of well-developed molecular fluorescence probes. Furthermore, the adaptability of this nano-array platform can be extended to other florescence probe system, suggesting its potential for detecting a wide range of signaling small molecules beyond H₂S.

Methods

Chemicals and characterization

Sodium bis(2-ethylhexyl) sulfosuccinate (AOT, MACKLIIN, 96%), Rhodamine (RB, Aladdin, >95.0% (HPLC)), β-Cyclodextrin (CD, Aladdin, 98%), Isooctane (Aladdin, 99%), cyclohexane (Shanghai Lingfeng Chemical Reagent Co. Ltd, ≥99.7%, AR), DMSO (Sinopharm Chemical Reagent Co., Ltd, 99.0%), CYTOP (ASAHI GLASS COMPANY, Japan), F1²⁺ (Deju Ye group, Nanjing University).

All chemicals were used as received without further purification.

Preparation of reverse micelle solutions[52]

The dye and F1²⁺ stock solutions were prepared by dissolving dye molecule (RB or 1:1 RB/CD) in water and F1²⁺ powders in water solution with a very small amount of DMSO, respectively. Then, F1²⁺/RB stock solution (molar ratio of 2:1) and F1²⁺/RB/CD stock solution (molar ratio of 2:1:1) were prepared with overall molecule concentration of 5.0 mM.

The reverse micelle solutions were prepared by injecting 10 μL aqueous stock molecular solution into 82.6 μL AOT/isooctane solution with ultrasonication until forming clear and transparent solution. The concentration of AOT/isooctane was fixed at 1.12 M and thus the ω value of micelle solutions was kept at 6.0. Prior to assembly, the micelle solution was diluted tenfold with cyclohexane.

Dynamic light scattering (DLS) and zeta potential measurements were performed on a 90 Plus/BI-MAS equipment (Brookhaven, USA).

Fabrication of molecule nano-array[42,43]

The molecule nano-array was fabricated by modifying electric field-assisted surface sorption nano-printing (EFASP) method which consists of two stpes: charge array writing on a fluorine polymer electret (CYTOP) and micelle assembly on the charged array.

In a typical process, fluorine polymer CYTOP was spin-coated on Si substrate which was pre-marked by lithography and baked to remove extra solvent for forming a 110 nm thick film (electret). Then, by applying high voltage (−40V to −90V) on a conductive AFM tip and writing charge on the electret film with pre-designed array pattern based on AFM scanning system, surface charge arrays (−0.15 to −3.0 V) were generated. At the same time, local surface modification occurs at the charged position, Kevin probe scanning (KPFM) measurements were determined whether the charge array was written successfully. All the charge writing process was performed in the air under ambient conditions (room temperature, relative humidity = 20–40%). The charge writing and KPFM scanning were performed on a NT-MDT AFM instrument.

After that, water-in-oil reverse micelle solution was dropped onto the charged area and tilted it after immersed 30 s. Micelles containing hybrid molecules were captured to the charged arrays locally. The morphology after micelle assemblies is characterized by the AFM tapping mode scanning.

Detection of hydrogen sulfide

A thin layer of CTYOP (10–30 nm) was spun on the assembled hybrid molecule nano-array to protect it from being rinsed off during the H₂S detection. The CYTOP concentration, spin speed, spin time, and acceleration were set as 2%, 7000 rpm, 1 min and 2000 r/min². There is no change in fluorescence image, including fluorescence intensity and spots position, before and after CYTOP covering.

NaHS aqueous solution was used to generate H₂S. The related chemical equilibrium was provided in supporting information. NaHS aqueous solution with different concentrations were first prepared

ranging from 0.1 fM to 1 µM and used immediately after preparation (less than 5 min). During the detection, NaHS aqueous solutions (10 µL) with different concentrations were dropped onto different molecular nano-arrays and blown away by N_2 stream after 2 min. Finally, The nano-arrays were placed on a home-made wide-field inverted fluorescence microscope and their fluorescence photos were taken at different times.

The fluorescence microscope was set up by Olympus inverted fluorescence microscope with PI spectrometer and Electron Multiplying Charge-Coupled Device (EMCCD). The 532 continuous-wave laser is fiber-coupled and focused on the focal plane behind the objective lens through a long focal length lens. After passing through the 60× objective lens, a spot of light about 100 microns in diameter focused on the sample. The emitted fluorescence is collected by an EMCCD after passing through the color filter with exposure time of 1 s. The power of the excited light is fixed at 30 µW.

The fluorescence intensity changes of $F1^{2+}$/RB/CD micelles towards NaHS in solution were also measured using FluoroMax-4 spectrofluorophotometer (HITACHI, Japan) with 532 nm laser as the excitation light source. The solution with a ratio of 2:1:1 for $F1^{2+}$/RB/CD was selected to form micelles. It was then diluted by a factor of 10 with cyclohexane, which is consistent with the preparation of nanoarrays. The fluorescence intensities at each NaHS concentration were measured after adding 10 uL (matching the amount of NaHS solution in nanoarray detection) of NaHS aqueous solution and ultrasonically forming a uniformly clarified micelle solution.

Data analysis

Image analysis was performed in MATLAB. Each original fluorescence image was calculated by subtracting the mean background value (M_{bg}) and all the background (light intensity below 20 after subtracting M_{bg}) was set to 0. We take these results as effective fluorescence images. Then we divided each effective fluorescence image into small images so that each small image contains one spot (Supplementary Figs. S5 and S7). We calculated the sum of fluorescence intensity (I_{sum}) of each spot. If the I_{sum} of a spot is larger than the average I_{sum} of spots before NaHS reaction, we considered it a illuminated spot ("on" spot). The average fluorescence intensity or the number of "on" spots were used to establish functional relationship with the concentration of NaHS, noted as INTEN and NUMB method, respectively.

Calibration curves were fit using a four-parameter logistic (4-PL) fit in Origin software. The values of fitting parameters are listed in Supplementary Table S1. A linear regression was applied to the steepest part of the calibration curve. The background level is defined as the negative control (identical procedures using water instead of NaHS solutions) plusing three times of the standard deviation. The intersection of the regression line and the background level defined the LOD.

Data availability

The data used and generated in this study have been deposited in the Figshare Database: https://doi.org/10.6084/m9.figshare.26965444. Source data (Figs. 2d, 3b, and 4b and Supporting Information Figs. S2a-b, S3a–b, S4a-b, S5, S6a-b, S7d-e, S8, S9, S11, and S14) are provided with this paper[53]. The authors declare that all other data are available from the corresponding author upon request.

References

1. Szabo, C. Hydrogen sulphide and its therapeutic potential. *Nat. Rev. Drug. Discov.* **6**, 917–935 (2007).
2. Das, A. et al. Impairment of an endothelial NAD(+)-H(2)S signaling network is a reversible cause of vascular aging. *Cell* **173**, 74–89 (2018).
3. Yang, G. et al. H2S as a physiologic vasorelaxant: hypertension in mice with deletion of cystathionine g-lyase. *Science* **322**, 587–590 (2008).
4. Kolluru, G. K., Shackelford, R. E., Shen, X., Dominic, P. & Kevil, C. G. Sulfide regulation of cardiovascular function in health and disease. *Nat. Rev. Cardiol.* **20**, 109–125 (2022).
5. Kolluru, G. K., Shen, X., Bir, S. C. & Kevil, C. G. Hydrogen sulfide chemical biology: pathophysiological roles and detection. *Nitric Oxide* **35**, 5–20 (2013).
6. Bae, S. K. et al. A ratiometric two-photon fluorescent probe reveals reduction in mitochondrial H2S production in Parkinson's disease gene knockout astrocytes. *J. Am. Chem. Soc.* **135**, 9915–9923 (2013).
7. Chen, H.-Y. et al. Cell membrane-targeted surface enhanced Raman scattering nanoprobes for the monitoring of hydrogen sulfide secreted from living cells. *Biosens. Bioelectron.* **250**, 116054 (2024).
8. Chen, Y. et al. A ratiometric fluorescent probe for rapid detection of hydrogen sulfide in mitochondria. *Angew. Chem. Int. Ed. Engl.* **52**, 1688–1691 (2013).
9. Du, Z. et al. Quantitative monitoring and visualization of hydrogen sulfide in vivo using a luminescent probe based on a ruthenium(II) complex. *Angew. Chem. Int. Ed. Engl.* **57**, 3999–4004 (2018).
10. Hammers, M. D. et al. A bright fluorescent probe for H2S enables analyte-responsive, 3D imaging in live zebrafish using light sheet fluorescence microscopy. *J. Am. Chem. Soc.* **137**, 10216–10223 (2015).
11. Lippert, A. R., New, E. J. & Chang, C. J. Reaction-based fluorescent probes for selective imaging of hydrogen sulfide in living cells. *J. Am. Chem. Soc.* **133**, 10078–10080 (2011).
12. Liu, Y. et al. Rationally designed pure-inorganic upconversion nanoprobes for ultra-highly selective hydrogen sulfide imaging and elimination in vivo. *Chem. Sci.* **10**, 1193–1200 (2019).
13. Ning, N. et al. Dysregulation of hydrogen sulphide metabolism impairs oviductal transport of embryos. *Nat. Commun.* **5**, 4107 (2014).
14. Qian, Y. et al. Selective fluorescent probes for live-cell monitoring of sulphide. *Nat. Commun.* **2**, 495 (2011).
15. Sasakura, K. et al. Development of a highly selective fluorescence probe for hydrogen sulfide. *J. Am. Chem. Soc.* **133**, 18003–18005 (2011).
16. Xu, G. et al. Imaging of colorectal cancers using activatable nanoprobes with second near-infrared window emission. *Angew. Chem. Int. Ed. Engl.* **57**, 3626–3630 (2018).
17. Zhao, C. et al. Forster resonance energy transfer switchable self-assembled micellar nanoprobe: ratiometric fluorescent trapping of endogenous H2S generation via fluvastatin-stimulated upregulation. *J. Am. Chem. Soc.* **137**, 8490–8498 (2015).
18. Wu, L. et al. H(2)S-activatable near-infrared afterglow luminescent probes for sensitive molecular imaging in vivo. *Nat. Commun.* **11**, 446 (2020).
19. Wu, L. et al. Engineering of electrochromic materials as activatable probes for molecular imaging and photodynamic therapy. *J. Am. Chem. Soc.* **140**, 16340–16352 (2018).
20. Guyon, I., Weston, J. & Barnhill, S. Gene selection for cancer classification using support vector machines. *Mach. Learn.* **46**, 389–422 (2002).
21. Chow, K.-F., Mavré, F. O., Crooks, J. A., Chang, B.-Y. & Crooks, R. M. A large-scale, wireless electrochemical bipolar electrode microarray. *J. Am. Chem. Soc.* **131**, 8364–8365 (2009).
22. LaFratta, C. N. & Walt, D. R. Very high density sensing arrays. *Chem. Rev.* **108**, 614–637 (2008).
23. MacBeath, G. & Schreiber, S. L. Printing proteins as microarrays for high-throughput function determination. *Science* **289**, 1760–1763 (2000).

24. Szunerits, S., Tam, J. M., Thouin, L., Amatore, C. & Walt, D. R. Spatially resolved electrochemiluminescence on an array of electrode tips. *Anal. Chem.* **75**, 4382–4388 (2003).

25. Zhang, J. et al. Localized electrochemiluminescence from nanoneedle electrodes for very-high-density electrochemical sensing. *Anal. Chem.* **89**, 11399–11404 (2017).

26. Lee, K., Kim, E., Mirkin, C. A. & Wolinsky, S. M. The use of nanoarrays for highly sensitive and selective detection of human immunodeficiency virus type 1 in plasma. *Nano Lett.* **4**, 1869–1872 (2004).

27. Blanco, E. M., Nesbitt, S. A., Horton, M. A. & Mesquida, P. A Multiprotein Microarray on Silicon Dioxide Fabricated by Using Electric-Droplet Lithography. *Adv. Mater.* **19**, 2469–2473 (2007).

28. Rosi, N. L. & Mirkin, C. A. Nanostructures in biodiagnostics. *Chem. Rev.* **105**, 1547–1562 (2005).

29. Cohen, L. & Walt, D. R. Single-molecule arrays for protein and nucleic acid analysis. *Annu. Rev. Anal. Chem.* **10**, 345–363 (2017).

30. Ginger, D. S., Zhang, H. & Mirkin, C. A. The evolution of dip-pen nanolithography. *Angew. Chem. Int. Ed. Engl.* **43**, 30–45 (2004).

31. Liu, G., Petrosko, S. H., Zheng, Z. & Mirkin, C. A. Evolution of dip-pen nanolithography (DPN): from molecular patterning to materials discovery. *Chem. Rev.* **120**, 6009–6047 (2020).

32. Huo, F. et al. Polymer pen lithography. *Science* **321**, 1658–1660 (2008).

33. Zhou, H., Li, Z., Wu, A., Wei, G. & Liu, Z. Direct patterning of rhodamine 6G molecules on mica by dip-pen nanolithography. *Appl. Surf. Sci.* **236**, 18–24 (2004).

34. Hyun, J., Kim, J., Craig, S. L. & Chilkoti, A. Enzymatic nanolithography of a self-assembled oligonucleotide monolayer on gold. *J. Am. Chem. Soc.* **126**, 4770–4771 (2004).

35. Braunschweig, A. B., Huo, F. & Mirkin, C. A. Molecular printing. *Nat. Chem.* **1**, 353–358 (2009).

36. Mesquida, P., Ammann, D. L., MacPhee, C. E. & McKendry, R. A. Microarrays of peptide fibrils created by electrostatically controlled deposition. *Adv. Mater.* **17**, 893–897 (2005).

37. Mesquida, P., Blanco, E. M. & McKendry, R. A. Patterning amyloid peptide fibrils by AFM charge writing. *Langmuir* **22**, 9089–9091 (2006).

38. Blanco, E. M., Nesbitt, S. A., Horton, M. A. & Mesquida, P. A multiprotein microarray on silicon dioxide fabricated by using electric-droplet lithography. *Adv. Mater.* **19**, 2469–2473 (2007).

39. Lee, K.-B., Park, S.-J., Mirkin, C. A., Smith, J. C. & Mrksich, M. Protein nanoarrays generated by dip-pen nanolithography. *Science* **295**, 1702–1705 (2002).

40. Demers, L. M. et al. Direct patterning of modified oligonucleotides on metals and insulators by dip-pen nanolithography. *Science* **296**, 1836–1838 (2002).

41. Taton, T. A., Mirkin, C. A. & Letsinger, R. L. Scanometric DNA array detection with nanoparticle probes. *Science* **289**, 1757–1760 (2000).

42. Xing, X. et al. Patterning of molecules/ions via reverse micelle vessels by nanoxerography. *ACS Appl. Mater. Inter.* **15**, 29542–29549 (2023).

43. Xing, X. et al. High-resolution combinatorial patterning of functional nanoparticles. *Nat. Commun.* **11**, 6002 (2020).

44. Wei, Y. et al. Turn-on fluorescence humidity sensing based on Cs4PbBr6 nanocrystal array. *J. Mater. Chem. C* **12**, 4054–4061 (2024).

45. Wei, Y. et al. Plasmon-Enhanced Electrochemiluminescence at the Single-Nanoparticle Level. *Angew. Chem. Int. Ed. Engl.* **62**, e202214103 (2023).

46. Zhang, Y. et al. Printed hybrid upconversion/perovskite nanoparticle cluster and its individual photoluminescence imaging. *Adv. Opt. Mater.* **11**, 2201841 (2022).

47. Man, Z., Bian, J., Xing, X., Lu, Z. & Zhang, W. Unexpected coulomb interactions in nonpolar solvent for highly efficient nanoxerography of perovskite quantum dots. *J. Phys. Chem. Lett.* **12**, 59–64 (2020).

48. Farka, Z., Mickert, M. J., Hlavacek, A., Skladal, P. & Gorris, H. H. Single molecule upconversion-linked immunosorbent assay with extended dynamic range for the sensitive detection of diagnostic biomarkers. *Anal. Chem.* **89**, 11825–11830 (2017).

49. Zang, F. et al. Ultrasensitive ebola virus antigen sensing via 3D nanoantenna arrays. *Adv. Mater.* **31**, 1902331 (2019).

50. Qiu, P. et al. Pushing the Limit of Ordered Mesoporous Materials via 2D Self-Assembly for Energy Conversion and Storage. *Adv. Funct. Mater.* **31**, 2007496 (2020).

51. Zhu, G. et al. Constructing Structurally Ordered High-Entropy Alloy Nanoparticles on Nitrogen-Rich Mesoporous Carbon Nanosheets for High-Performance Oxygen Reduction. *Adv. Mater.* **34**, 2110128 (2022).

52. Wu, M. L., Chen, D. H. & Huang, T. C. Synthesis of Au_Pd Bimetallic Nanoparticles in Reverse Micelles. *Langmuir* **17**, 3877–3883 (2001).

53. Xing, X. et al. Femtomolar Hydrogen Sulfide Detection via Hybrid Small-Molecule Nano-arrays. figshare. Dataset. https://doi.org/10.6084/m9.figshare.26965444 (2024).

Acknowledgements

Author contributions

Z.L., D.Y., W.Z., and X.X. conceptualized and designed the research. X.X. performed the experiments and wrote the original draft. L.W. and D.Y. provided reagents and expertise and participated in research discussion. Y.I. and T.S. synthesized F1²⁺ molecules. Y.Z., J.P., H.X., J.Z., W.Z., and Z.L. provide measurement support. Z.L. contributes to the review & editing process. Z.L. and X.X. provided funding for project. All authors discussed the results and commented on the manuscript.

Competing interests

The authors declare no competing interests.

Additional information

Supplementary information The online version contains supplementary material available at https://doi.org/10.1038/s41467-024-55123-y.

Correspondence and requests for materials should be addressed to Zhenda Lu.

Peer review information *Nature Communications* thanks Pengpeng Qiu and the other, anonymous, reviewer(s) for their contribution to the peer review of this work. A peer review file is available.

Reprints and permissions information is available at http://www.nature.com/reprints